Nanoscale compositional mapping with gentle forces

Microscopists have always pursued the development of an instrument that combines topography and materials properties analyses at the highest resolution. The measurement of the tiny amount of energy dissipated by a vibrating tip in the proximity of the sample surface has provided atomic force microscopes with a robust and versatile method to determine the morphology and the compositional variations of surfaces in their natural environment. Applications in biology, polymer science and microelectronics illustrate the potential of phase-imaging force microscopy for nanoscale analysis.

RICARDO GARCÍA[1], ROBERT MAGERLE[2] AND RUBEN PEREZ[3]

[1]Instituto de Microelectrónica de Madrid, CSIC, 28760 Tres Cantos, Madrid, Spain
[2]Chemische Physik, Technische Universität Chemnitz, D-09107 Chemnitz, Germany
[3]Departamento de Física Teórica de la Materia Condensada, Universidad Autónoma de Madrid, 28049 Madrid, Spain

e-mail: rgarcia@imm.cnm.csic.es

Soft and bio-inspired materials as well as biomolecules are attracting growing interest within the materials science community. Characterization of those materials in their natural environment requires new microscopic tools that combine topography and compositional mapping at the highest resolution and sensitivity[1–4]. Amplitude-modulation atomic force microscopy (AM-AFM), often known as tapping-mode AFM, has opened a variety of ways to image, in a gentle, non-destructive manner and with high spatial resolution, heterogeneous materials in their natural environment and state. Today, polymers, cell membranes and biomolecule aggregates as well as nanoelectronic devices are routinely imaged with sub-10-nm spatial resolution[5–8]. Molecular resolution has also been achieved in ambient conditions by using high-resolution probes[9].

A unique feature of AM-AFM is the ability to map simultaneously the shape and the compositional variations of the specimen's surface. These variations are measured by the phase lag of the vibrating probe with respect to the external excitation, technically known as phase imaging[10–12]. It has been demonstrated that the three-dimensional cantilever-probe motion can be understood in terms of point-mass models[13–15]. This enables the reconstruction of both the conservative and dissipative tip–surface forces from the oscillation amplitude and the phase-shift dependence on the average tip–surface separation[16–18]. Specifically, the transformation of phase-shift measurements into energy-dissipation values enables experimental data to be linked to materials properties such as stiffness, elasticity, viscosity or surface-adhesion energy, which in turn opens the way to a quantitative nanoscale spectroscopy compatible with technological environments[19]. A better understanding of the sources of noise in the optical detection system and its effects on the probe motion have also improved the signal-to-noise ratio while minimizing tip–surface forces[20,21]. Those developments are compatible with data-acquisition times reaching video rates[22–24], which, in turn,

will enable the study of a wide variety of dynamical processes with unprecedented temporal and spatial resolution while providing quantitative information about material properties.

SEPARATION OF TOPOGRAPHY AND COMPOSITION

In AM-AFM a sharp probe (tip) placed a few nanometres above the sample surface is mechanically excited at a fixed frequency, usually near or at the first flexural resonance frequency[8]. The probe–surface interaction forces lead to a reduction of the amplitude of the oscillation from its free value. Any kind of interaction existing between tip and sample independent of either its physical origin (electrostatic, van der Waals or chemical adhesion) or nature (short-range versus long-range interactions) will reduce the amplitude (Box 1). In this imaging technique, the amplitude is used as a feedback parameter to map the topography of the surface. The net value of the force exerted by the tip on the sample surface, either positive or negative, defines two different imaging regimes, repulsive or attractive, respectively. The force exerted on the sample depends on several factors such as the free amplitude, the tip's radius, the value of the amplitude chosen to run the feedback or the imaging regime. Maximum forces below 1 nN (peak value) have been achieved by using free amplitudes of a few nanometres (5–10 nm) and sharp silicon tips (~2–5 nm). Those forces are required to non-destructively image weakly adsorbed biomolecules deposited on flat supports[8,25].

For several years, AM-AFM experimental data was mostly explained in terms of numerical simulations[8,26,27]. This trend is rapidly changing because several theoretical approximations have overcome the mathematical difficulties posed by the nonlinear dynamics of the tip motion[16–18,28,29]. The key assumptions are considering the cantilever-tip system as a driven anharmonic oscillator with damping, and performing averages over the oscillation period. Those approximations make it possible to express tip–surface conservative and dissipative forces in terms of observable features such as amplitudes or phase shifts.

A mechanically driven oscillation is characterized by three parameters, the amplitude, the frequency and the phase lag with respect to the mechanical excitation. In AM-AFM, the excitation frequency is fixed at the beginning of the experiment, whereas the amplitude and the phase lag of the oscillation provide two channels to explore tip–surface conservative (elastic) and dissipative (inelastic)

Box 1 AM-AFM with topography and compositional sensitivity

In AM-AFM a topographic image is generated by scanning the tip across the surface while keeping the oscillating amplitude fixed (Fig. 1). The application of the virial theorem to the tip motion enables a relationship to be derived between the amplitude A and the average value of the conservative tip–surface forces $\langle Fts \rangle$ (ref. 17)

$$A \approx A_0 \left[1 - 4 \left(\frac{\langle F_{ts} \rangle}{F_0} \right)^{1/2} \right]. \qquad (1)$$

Equation 1 shows that any type of conservative force will reduce the amplitude from its free value (A_0). This equation is only valid for $\omega = \omega_0$, where ω is the driving frequency and ω_0 is the free resonance frequency. F_0 is the external force that drives the tip oscillation.

Separation of topography and composition arises because in the steady-state operation of the microscope ($z = z_0 + A\cos(\omega t - \phi)$; t is time) the average energy released by the cantilever to the medium E_{med} (air or liquid) and the sample surface must match the average energy supply by the external driving force. Then, the phase-shift lag ϕ between the microcantilever excitation and the probe's response is related to the oscillation amplitude A and the average energy dissipated in the sample E_{dis} and in the environment E_{med} by $\omega = \omega_0$ (ref. 39)

$$\sin\phi = \frac{A}{A_0} \left(1 + \frac{E_{dis}}{E_{med}} \right). \qquad (2)$$

The prefactor (A/A_0) and E_{med} remain constant during AM-AFM imaging (A = constant). Consequently, any change of the phase shift is directly related to a local change in the energy dissipated in the sample and independent of the topography. The oscillation amplitude is kept constant by the feedback system with only small instantaneous variations because of the finite response of the electronics. The influence of those variations on the phase shift is negligible in first approximation. The phase shift of the oscillation with respect to a reference value tracks composition variations.

In liquids, where the quality factor of the cantilever is small ($Q \sim 1 – 5$), the higher harmonic components of the oscillation amplitude could have a non-negligible contribution on the tip motion[13,60]. In this case, equation (2) should be modified, in particular when the first two harmonics (A_1, A_2) are the main components of the oscillation, $z = z_0 + A_1\cos(\omega t - \phi_1) + A_2 \cos(2\omega t - \phi_2)$, it can be shown that $\omega = \omega_0$,

$$\sin\phi_1 = \frac{A_1}{A_0} \left(1 + 4 \frac{A_2^2}{A_1^2} + \frac{E_{dis}}{E_{med}} \right). \qquad (3)$$

Equation 3 is derived by applying a methodology similar to the one used to obtain equation (2). The above result says that for small Q values, a complete separation between topography and dissipation is not possible. Nonetheless, equation (2) still remains a good approximation whenever $A_1 \geq 40A_2$. This is usually the case in many AFM experiments in liquids.

interactions. In general, those channels are coupled, that is, they are modified by the same type of tip–surface properties, however, they may be decoupled by operating the instrument at a fixed amplitude (see Fig. 1). Any topographic variation will modify the tip–surface distance and as a consequence will induce an instantaneous change of the amplitude. However, a feedback mechanism will keep the amplitude constant by adjusting the vertical z position of the sample holder to compensate for the topography. This process is performed while the vibrating tip is displaced across the sample surface. A topographic image is generated by recording this vertical z movement. Separation of topography and composition from the experimental signal is achieved by recording and plotting independently the vertical z displacement of the sample base (topography) and the phase lag of the tip vibration (composition).

PHASE IMAGING, ENERGY DISSIPATION AND COMPOSITIONAL CONTRAST

The phase lag between the external excitation of the vibrating probe and its response to the tip–surface interactions, referred to as phase shift, is related to the local energy dissipation on the surface[11,19,30–40]. Specifically, the sine of the phase shift ϕ is proportional to the amount of inelastic energy transferred from the tip to the sample surface (equation (2) in Box 1). Although energy dissipation is often associated with irreversible sample deformation, in AM-AFM the energy could be dissipated in a gentle and non-invasive manner that does not involve sample modification and, therefore, it is compatible with nanoscale spatial resolution. As in the case of the exerted force in the sample, the value of the dissipated energy depends on both experimental parameters and tip–sample inelastic processes. Typical high-resolution experiments involve dissipated values per cycle in the 0.5–50 eV range. For a spatial resolution of 2 nm, those values imply

a dissipated energy per bond that ranges from 0.001 to 0.1 eV, that is, far less than the bonding energies of most materials.

The qualitative advantages of mechanical phase imaging have been recognized and exploited quite early[10–12], however, quantitative measurements of materials properties have been hampered by several factors, among them, the complexity of the dynamics experienced by the vibrating probe and the insufficient knowledge of the shape of the tip. This is about to change because recent contributions are shedding light onto the relationships between nonlinear dynamics, tip–surface forces and energy-dissipation processes during imaging[15–19], and new microfabrication processes are delivering AFM tips with more controllable geometries and surface properties (see catalogues from manufacturers of AFM cantilevers).

Dissipation in AFM can be described at the molecular or nanoscale level. At the molecular level, the emphasis is placed on the specific atomic processes that enable the transfer of mechanical energy to atomic and molecular motions in the sample[5,41,42]. The atomistic and molecular mechanisms responsible for dissipation depend on both materials properties and the environment. They may involve force-induced stable atomic bonding configurations or molecular reorientations, interdigitation, exchange of atoms and molecules or charged-induced dissipation effects. At the nanoscale, the emphasis is placed on the quantitative relationship between dissipation processes such as surface-adhesion hysteresis, viscoelasticity, friction or long-range dissipative interfacial interactions and macroscopic quantities such as surface-adhesion energy, elastic modulus, stiffness, plasticity index or viscosity coefficient[19,38–40,43]. In many cases, analytical relationships between the measured dissipation values (phase shifts) and sample properties have been derived (Fig. 2). Those expressions have enabled the transformation of experimental phase-shift values into measurements of materials properties (see Box 2).

Phase-imaging experiments are not the only methods used in the quest for quantitative nanoscale analysis. Several micro- and nanorheology[44,45] methods can be used as a benchmark for quantitative measurements on polymers, whereas the damping of the oscillation amplitude in a related AFM method (frequency modulation AFM) also offers a source of contrast at the atomic level in ultra-high-vacuum environments[5,42].

FROM LIVING CELLS TO NANOELECTRONIC CIRCUITS

The generality of the physical principles responsible for phase-imaging contrast makes it possible to image a large variety of materials with micrometre, submicrometre or nanoscale features in either air or liquids. The materials range from polymer surfaces, cells, carbon nanotubes, self-assembled monolayers and liquid droplets to nanoscale electronic devices[19,46–51]. In fact, the same instrument may be used to image all of the above materials. The localization of the dissipation process has also enabled surface proteins to be imaged with 1.4-nm lateral resolution[34], as well as protein–DNA interactions in liquids[52]. Imaging living biomolecules just requires the use of fluid cells that are readily incorporated into a force microscope. Figure 3 shows several examples of the materials imaged in different environments, in their native state and with no major preparation protocols such as staining or fixation.

Phase imaging can achieve nanometre-scale resolution on biological samples under native conditions and at scanning speeds reaching video rates. An assembly of chaperonins GroEL — protein complexes that assist the folding of linear amino acid chains into functional proteins — are shown in Fig. 3a. The phase image shows the molecular structure of the GroEL in liquid and it resolves the seven monomers of the top ring of the GroEL as well as its central cavity[53].

Fabrication and full characterization of nanoelectronic circuits represent one of the key challenges in nanotechnology. Figure 3b shows an image of an etch mask used for the fabrication of 5-nm interdigitated nanowires. After wet etching in hydrogen fluoride, the phase image enables density variations and discontinuities to be resolved with 3-nm spatial resolution in the interdigitated lines. Because density variations may not imply changes in the morphology, they are not detected in the topography image.

Imaging wood pulp fibre illustrates both the variety of materials accessible to phase imaging as well as its technological relevance as a characterization tool for rough surfaces. Figure 3c,d shows the topography and the phase image of a wood pulp fibre[10]. The topography (Fig. 3c) shows height variations in the micrometre range, which makes it hard to perceive nanoscale structures. Furthermore, the topography image is uninformative about the heterogeneous composition of the sample surface. In contrast, the phase image (Fig. 3d) reveals both the structure and the composition of the wood fibre. The cellulose microfibrils are clearly resolved in spite of the roughness of the surface; the white spots in the phase image reveal the presence of deposits made of amorphous lignin. The identification of lignin patches helps to develop efficient and low-pollution methods for producing white paper.

Topography and phase images can be combined to produce a complete three dimensional characterization of the sample surface by providing simultaneous information on structure, composition and height variations, which enables the phase behaviour of thin films to be described in terms of surface reconstructions[54]. Figure 4 shows the complex phase structure of a triblock copolymer: polystyrene–polybutadiene–polystyrene (SBS) film. The image shows how the microdomain structure depends on the film thickness. The upper terrace shows the polystyrene (PS) cylinders oriented parallel to the surface. In the thinner regions of the film (bottom terraces) two patterns are found. One terrace is characterized by hexagonally
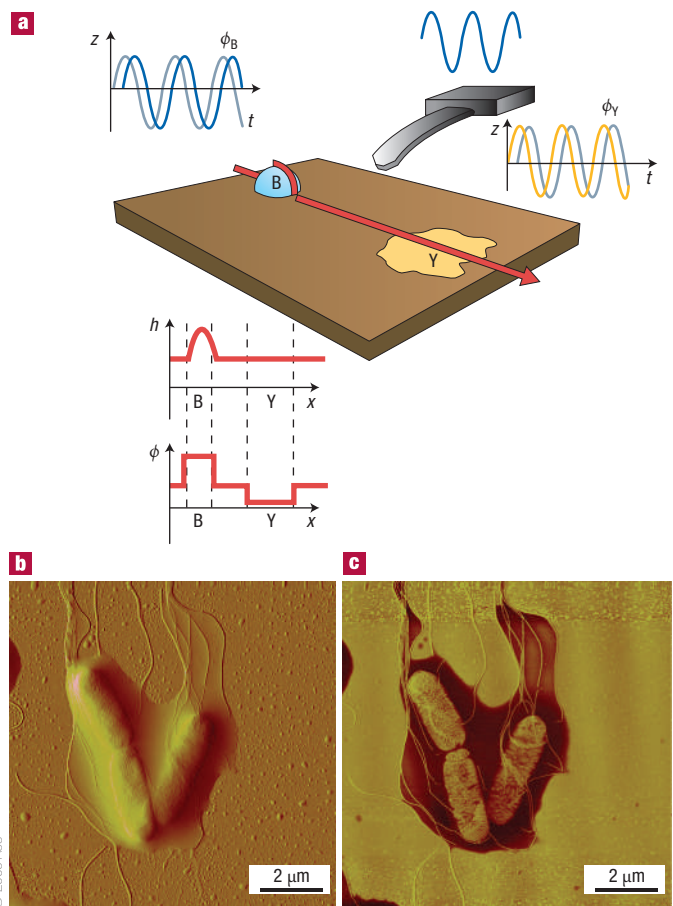
Figure 1 Introducing AM-AFM. **a**, Scheme of the phase-imaging operation. The cantilever oscillation depends on the topography and its composition. The phase-shift signal in AM-AFM only changes with variation in the dissipated energy on the sample surface. The image shows two different local regions on the flat substrate (brown). The blue region (B) is made of a different material, and protrudes from the substrate baseline. The yellow region (Y) is flat and shows only changes in materials properties. The blue region will image in the height (h) signal (topography), whereas the yellow region will not appear in the height trace. However, both regions will be clearly distinguished from the substrate by recording and plotting the phase signal (ϕ). **b,c**, The above considerations are illustrated by comparing the topography of an aggregate of three *Salmonella typhimurium* cells covered by an extracellular polymeric capsule (**b**) and the phase image (**c**), that is acquired simultaneously with the topography, reveals the inner structure of the cell as well as the continuity of the flagellae. (R. Avci *et al.* ref. 49 © 2007 American Chemical Society).

ordered dark spots, indicative of a hexagonal PS lamella phase. In the other terrace, which is the thinnest, the polystyrene cylinders are oriented parallel to the surface as in the upper terrace. The slope between terraces displays a hexagonal pattern of bright dots, indicative of PS cylinders oriented perpendicular to the surface. The contrast (bright versus dark regions) in Fig. 4 comes from the phase signal; the z position at constant oscillation amplitude provides the height difference between terraces.

REAL-TIME AND THREE-DIMENSIONAL IMAGING

Static microscopic images provide limited information about nanoscale dynamic processes. The compatibility of mechanical phase imaging with operation in liquids, application of gentle forces and
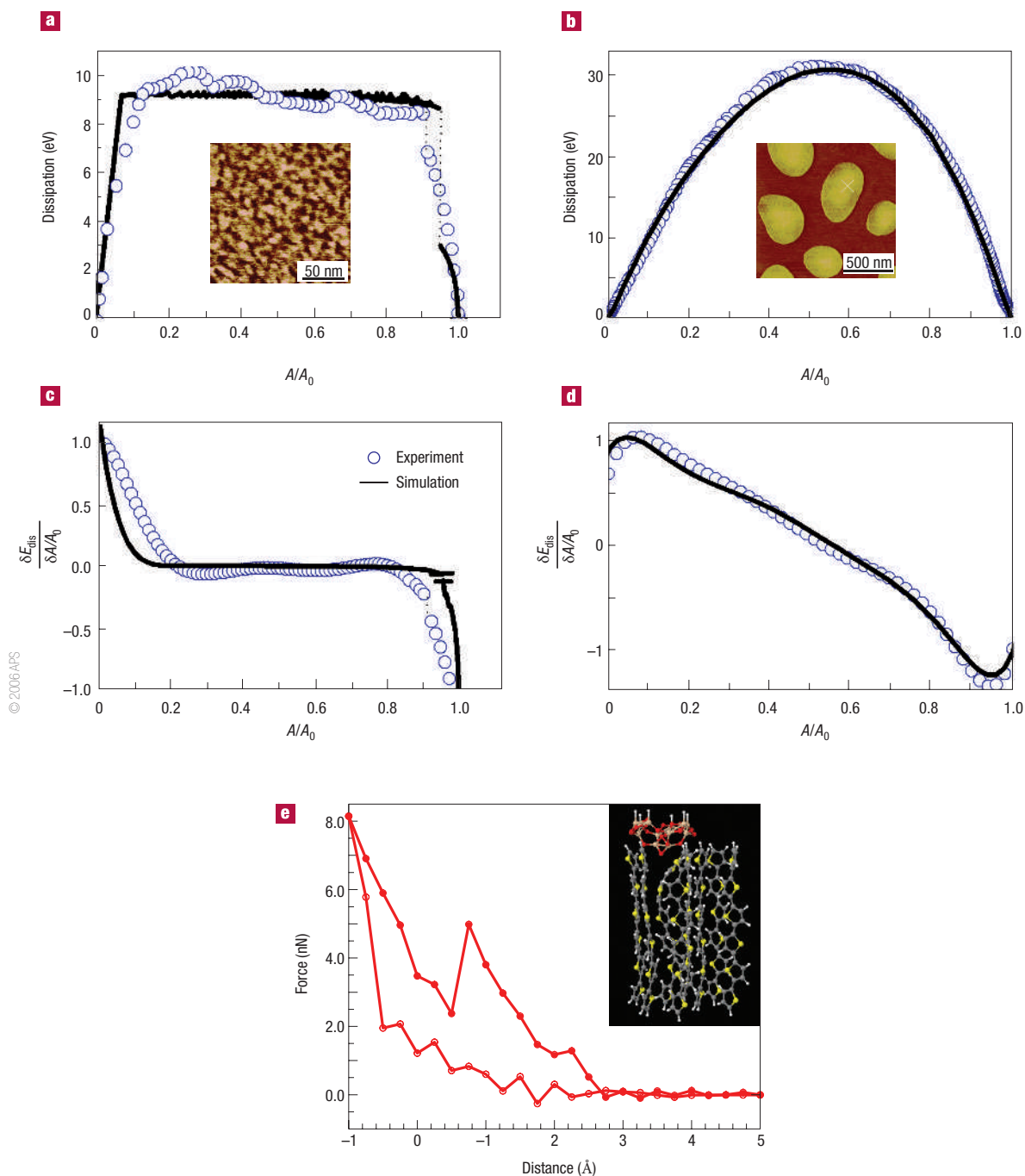
Figure 2 Energy dissipation curves. **a**, Measured and simulated dynamic-dissipation curves on silicon when there is surface-energy hysteresis and long-range interfacial interactions. **b**, Measured and simulated dynamic-dissipation curves on a polystyrene region of a polystyrene/polybutadiene blend. **c,d**, The derivatives of the normalized energy-dissipation curves shown in **a** and **b** respectively. The insets show the energy dissipation images taken on Si and on a PS region. Reprinted, in part, with permission from ref. 19. **e**, Calculated force-versus-distance curves for tip approach and retraction (open circles) at 0 K. The area enclosed by the force curves gives the energy dissipated (~7 eV). The inset shows the deformations induced by the interaction of a silicon oxide tip and a sexithiophene monolayer calculated with large-scale *ab initio* total energy methods. (Inset image courtesy of W. Kaminski and R. Perez).

fast data acquisition times enable the *in situ* study of several dynamic processes such as conformational changes of myosin after release of adenosine triphosphate[22], crystallization, melting and phase transitions in nanostructured polymeric fluids[54,55] or the motion of structural defects in block-copolymer melts[56–58].

Figure 5a–d shows a temporal sequence of the crystallization of a chiral random copolymer[59]. The images show how a single lamella changes its orientation during growth. After the leading edge-on lamellae have grown to a certain length (~2 µm) they bend anticlockwise towards the tangential direction. Then, they twist to

Box 2 Nanoscale energy dissipation and sample properties

The sine of the phase lag between the external excitation and the tip response is directly linked to the amount of energy dissipated on the sample (equation (2) in Box 1). On the other hand, several analytical relationships between the dissipation and sample properties such as surface adhesion energy, elastic modulus, stiffness, plasticity index or viscoelasticity have been derived[19]. For example, let's take the case of a dissipative process characterized by surface adhesion hysteresis, that is, when the work needed to separate two surfaces is always greater than that originally gained by bringing the surfaces together. Then the dissipated energy is proportional to differences in surface energies,

$$E_{dis} = F_{DMT}dz = \int 4\pi R\delta(\gamma_r - \gamma_a) , \qquad (4)$$

where δ is the deformation (indentation) and F_{DMT} is the Derjaguin–Muller–Toporov (DMT) forces in approach and retraction half periods; γ_r and γ_a are respectively the approach and retraction surface energies and R is the tip radius. Equations 2 and 4 allow the observer to turn AM-AFM observables such as phase shifts into material properties. Figure 2 shows the agreement obtained between experiments and theory for two different inelastic processes, surface adhesion hysteresis and viscoelasticity.

Ultimately, any dissipation process can be described by the existence of hysteresis in the force-versus-distance curve, that is, the force when the tip approaches the surface differs from the force when the tip retracts from the surface. At the atomic scale *ab initio* calculations show how this hysteresis is linked with the molecular deformations induced by the forces between the tip and the molecules. These force difference is described at the nanoscale by the hysteresis in the adhesion energy.

---

become flat-on lamellae and keep twisting to reveal an edge-on-view. Continuous twisting of lamellae seems to be the same everywhere in the imaged area. Although the twist of the individual lamellae is apparent in these surface images, the detailed three-dimensional shape is hard to infer from them.

This limitation of AFM to explore exclusively the surface of three-dimensional objects may be overcome with a layer-by-layer imaging approach[47], which enables the inner structure of a material to be imaged. This nanotomography approach combines alternating steps of etching and phase imaging. Etching can be performed *in situ* in the AFM chamber. The end result is a series of images from which the three-dimensional material can be reconstructed. Nanotomography has been applied to reveal the detailed microstructure of block copolymers, semicrystalline polymers, metallic superalloys and human bone. Using this method, the structural details of the twisting crystals shown in Fig. 5a–d could be resolved.

PERSPECTIVES

In nanometre-scale science and technology, a main aim is for a multipurpose tool for quantitative analysis of materials in technologically relevant environments (air or liquids), with no impact on the sample surface and with 1-nm spatial resolution. This context has stimulated the emergence of several methods based on electrical, optical or mechanical principles as well as several combinations of them. Currently, tools based on mechanical interactions provide the best compromise between spatial resolution, compositional sensitivity, wide range of applications and reliability. The control and measurement of the tiny amount of energy dissipated by a vibrating tip in the proximity of the sample surface has turned phase imaging into a robust and versatile method for quantifying the morphology and some materials properties of relevant surfaces in biology, polymer science and microelectronics with sub-10-nm resolution. To turn phase imaging with AFM into a multipurpose tool for topographic and compositional analysis with 1-nm spatial resolution is closely related to key technical advances in scanning probe technology, as well as progress in the fundamental understanding of the energy-dissipating interactions between nanoscale objects.

Key technical developments in scanning probe microscopy are focused on increasing image acquisition rates, reduction of the cantilever-tip size, preparation of ultrasharp and chemically stable tips, and development of multimodal resonant cantilevers. High-speed imaging will enable a wider range of dynamic processes to be explored
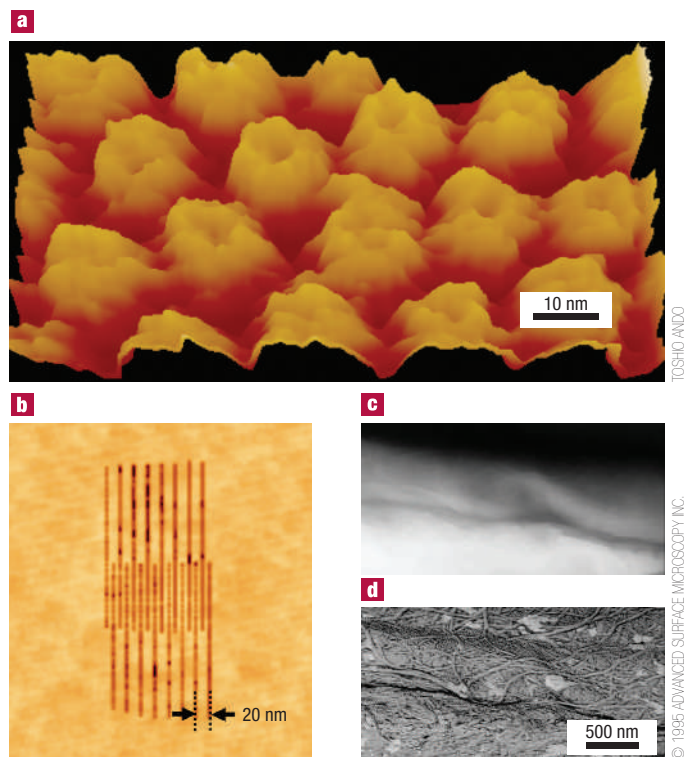
Figure 3 AFM phase-imaging. **a**, High-speed AFM phase images of an assembly of GroEL proteins in buffer solution. (Courtesy of T. Ando and T. Uchihashi). **b**, Phase image of an etch mask of 4-nm interdigitated lines. After wet etching in HF, the interdigitated lines show variations in the composition density (light and dark regions). Phase imaging enables compositional variations to be detected with 3-nm spatial resolution, which are otherwise unnoticeable in the topography image (not shown). (Courtesy of R.V. Martinez and R. Garcia). **c,d**, Topography (**c**) and phase image (**d**) of the same region of a wood-pulp fibre. The topography shows height variations of thousands of nanometres over square micrometre regions. This makes it very hard to detect nanometre-scale features. The phase image enables the structure of the cellulose microfibrils to be resolved with 30-nm resolution, and also provides compositional contrast by separating the cellulose from the lignin deposits (white spots in the image). Image courtesy of D. A. Chernoff.

© 2006 ACS

1 µm

Figure 4 Complex microdomain structure of a block copolymer. The AFM images are rendered into three-dimensions using the height image as height-field and the phase image as contrast. The images show the formation of terraces in a thin film of SBS block copolymer and the systematic change of microdomain structures along the changes in film thickness from 32 nm at the lowest terrace to 57 nm at the higher terrace. Reprinted with permission from ref. 54.

© 2006 ACS

1 µm
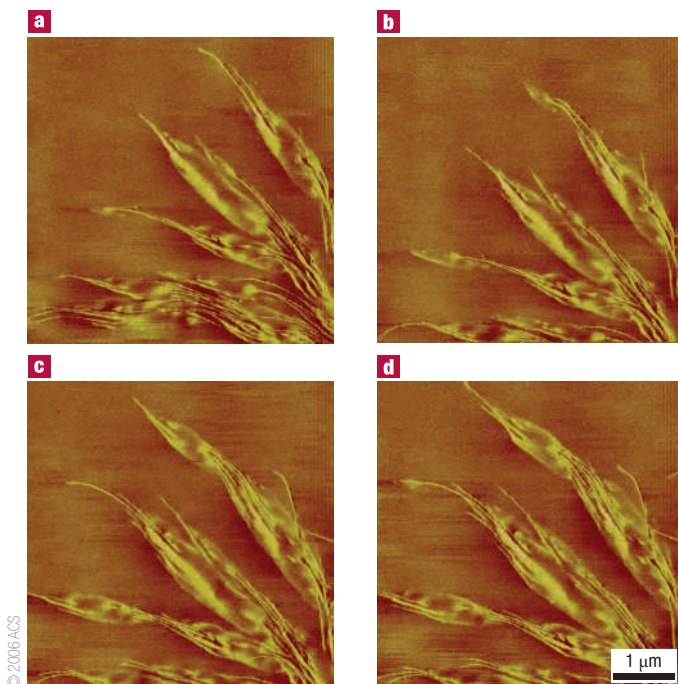
Figure 5 Real-time phase images of crystal twisting during the crystallization of a chiral random copolymer at 75 °C. **a**–**d**, The crystal after 0, 6, 18 and 24 minutes, respectively. Bright corresponds to hard crystalline regions, dark to soft amorphous matrix. Reprinted with permission from ref. 59.

in biology and materials sciences as well as reducing observation times in general. Smaller cantilever-tip systems will enable high resonance frequencies and small force constants while reducing the

hydrodynamic damping in liquids. Sharp and chemically stable tips are required for both high resolution and to ensure the reproducibility needed for quantitative measurements. A cantilever with several eigenmodes will provide different channels for separating tip–surface interaction processes. All these developments should be compatible with each other and, as a key requirement, exert only sub-1-nN forces between tip and sample surface. Such small forces are needed to observe dynamic processes or the structure of nanoscale molecules without introducing perturbations and/or deformations.

Equally important are the steps taken to understand how and what materials properties manifest themselves in terms of observable parameters such as amplitude reduction or phase shifts. Atomistic modelling and continuous theoretical approaches are both needed to be able to give a complete description of nanomechanical phenomena. The models should be able to explain nanoscale measurements in terms of macroscopic parameters such as surface adhesion energies, elastic modulus or viscoelastic coefficients.

Phase imaging offers nanoscale spatial resolution and high sensitivity for detecting compositional variations in native conditions, such as in air and aqueous solutions. Spatial resolution and compositional sensitivity are prompting the application of phase imaging to study new materials and phenomena, in particular, when dynamic processes are involved, or the characterization of heterogeneous materials made of regions with different chemical, structural or mechanical properties.

References

1. Jung, T. A., Himpsel, F. J., Schlittler, R. R. & Gimzewski, J. K. in *Scanning Probe Microscopy* (ed. Wiesendanger, R.) 11–48 (Springer, Berlin-Heidelberg 1998).
2. Hillenbrand, R., Taubner, T. & Keilmann, F. Photon-enhanced light–matter interaction at the nanometre scale. *Nature* **418**, 159–162 (2002).
3. Stroh, C. *et al.* Single-molecule recognition imaging-microscopy. *Proc. Natl. Acad. Sci. USA* **101**, 12503–12505 (2004).
4. Martinez, N. F., Patil, S., Lozano, J. R. & García, R. Enhanced compositional sensitivity in atomic force microscopy excitation of the first two flexural modes. *Appl. Phys. Lett.* **89**, 153115 (2006).
5. Meyer, E., Hug, H. J. & Bennewitz, R. *Scanning Probe Microscopy: Lab on a Tip* (Springer, Berlin, 2004).
6. Morita, S., Wiesendanger, R. & Meyer, E. (eds) *Noncontact Atomic Force Microscopy* (Springer, Berlin, 2002).
7. Jena, B. P. & Horber, J. K. H. *Atomic Force Microscopy in Cell Biology* (Academic Press, San Diego, 2002).
8. Garcia, R. & Perez, R. Dynamic atomic force microscopy methods. *Surf. Sci. Rep.* **47**, 197–301 (2002).
9. Klinov, D. & Magonov, S. True molecular resolution in tapping-mode atomic force microscopy. *Appl. Phys. Lett.* **84**, 2697–2699 (2004).
10. Chernoff, D. A. in *Proc. Microscopy and Microanalysis* (Bailey, G. W. *et al.* eds) 888–889 (Jones & Begell, New York, USA, 1995).
11. Tamayo, J. & García, R. Effects of elastic and inelastic interactions on phase contrast images in tapping-mode scanning force microscopy. *Appl. Phys. Lett.* **71**, 2394–2396 (1997).
12. Magonov, S. N., Elings, V. & Papkov, V. S. AFM study of thermotropic structural transitions in poly (diethylsiloxane). *Polymer* **38**, 297–307 (1997).
13. Rodriguez, T. R. & García, R. Tip motion in amplitude modulation (tapping-mode) atomic-force microscopy: comparison between continuous and point-mass models. *Appl. Phys. Lett.* **80**, 1646–1648 (2002).
14. Legleiter, J., Park, M., Cusik, B. & Kowalewski, T. Scanning probe acceleration microscopy in fluids: Mapping mechanical properties of surfaces at the nanoscale. *Proc. Natl Acad. Sci. USA* **103**, 4813–4818 (2006).
15. Hu, S. & Raman, A. Chaos in atomic force microscopy. *Phys. Rev. Lett.* **96**, 036107 (2006).
16. Lee, M. & Jhe, W. General theory of amplitude-modulation atomic force microscopy. *Phys. Rev. Lett.* **97**, 036104 (2006).
17. SanPaulo, A. & García, R. Tip-surface forces, amplitude, and energy dissipation in amplitude-modulation force microscopy. *Phys. Rev. B* **64**, 193411 (2001).
18. Hölscher, H. Quantitative measurement of tip-sample interactions in amplitude modulation AFM. *Appl. Phys. Lett.* **89**, 123109–123111 (2006).
19. García, R. *et al.* Identification of nanoscale dissipation processes by dynamic atomic force microscopy. *Phys. Rev. Lett.* **97**, 016103 (2006).
20. Fukuma, T., Kimura, M., Kobayashi, K., Matsushige, K. & Yamada, H. Development of low noise cantilever deflection sensor for multienvironment frequency-modulation AFM. *Rev. Sci. Instrum.* **76**, 053704 (2005).
21. Schäffer, T. E. Calculation of thermal noise in an atomic force microscope with a finite optical spot size. *Nanotechnology* **16**, 664–670 (2005).
22. Ando, T. *et al.* High-speed AFM for studying the dynamic behaviour of protein molecules at work. *Jpn J. Appl. Phys.* **45**, 1897–1903 (2006).
23. Humphris, A. D. L., Miles, M. J. & Hobbs, J. K. A mechanical microscope: High speed atomic force microscopy. *Appl. Phys. Lett.* **86**, 034106 (2005).
24. Hansma, P. K., Schitter, G., Fantner, G. E. & Prater C. High-speed atomic force microscopy. *Science* **314**, 601–602 (2006).

25. Thomson, N. H. The substructure of immunoglobulin G resolved to 25 kDA using amplitude modulation in air. *Ultramicroscopy* **105,** 1003–110 (2005).

26. Stark, M., Stark, R. W., Heckl, W. M. & Guckenberger, R. Inverting force microscopy: From signals to time-resolved interaction forces. *Proc. Natl Acad. Sci. USA* **99,** 8473–8478 (2002).

27. Kutana, A., Giapsis, K. P., Chen, J. Y. & Collier, C. P. Amplitude response of single-wall carbon nanotube probes during tapping mode atomic force microscopy: Modeling and experiment. *Nano Lett.* **6,** 1669–1673 (2006).

28. Balantekin, M. & Atalar, A. Power dissipation analysis in tapping-mode atomic force microscopy. *Phys. Rev. B* **67,** 193404 (2003).

29. Sahin, O., Quate, C. F., Solgaard, O. & Atalar, A. Resonant harmonic response in tapping-mode atomic force microscopy. *Phys. Rev. B* **69,** 165416 (2004).

30. Martin, P., Marsaudon, S., Aimé, J. P. & Bennetau, B. Experimental determination of conservative and dissipative parts in the tapping mode on a grafted layer: comparison with frequency modulation data. *Nanotechnology* **16,** 901–907 (2005).

31. Cleveland, J. P., Anczykowski, B., Schmid, A. E. & Elings, V. B. Energy dissipation in tapping-mode atomic force microscopy. *Appl. Phys. Lett.* **72,** 2613–2615 (1998).

32. Bar G *et al.* Factors affecting the height and phase images in tapping mode atomic force microscopy. Study of phase-separated polymer blends of poly(ethene-co-styrene) and poly(2,6-dimethyl-1,4-phenylene oxide). *Langmuir* **13,** 3807–3812 (1997).

33. Anczykowski, B., Gotsman, B., Fuchs, H., Cleveland, J. P. & Elings, V. B. How to measure energy dissipation in dynamic mode atomic force microscopy. *Appl. Surf. Sci.* **140,** 376–382 (1999).

34. Stark, M., Möller, C., Müller, D. J. & Guckenberger, R. From images to interactions: High-resolution phase imaging in tapping-mode AFM. *Biophys. J.* **80,** 3009–3018 (2001).

35. D'Amato, M. J., Markus, M. S., Eriksson, M. A. & Carpick, R. W. Phase imaging and the lever-sample tilt in dynamic atomic force microscopy imaging. *Appl. Phys. Lett.* **85,** 4738–4740 (2004).

36. Bodiguel, H., Montes, H. & Fretigny, C. Depth sensing and dissipation in tapping mode atomic force microscopy. *Rev. Sci. Instrum.* **75,** 2529–2535 (2004).

37. Kasai, T, Bhushan, B., Huang, L, & Chanmin, S. Topography and phase imaging using torsional resonance mode. *Nanotechnology* **15,** 731–742 (2004).

38. Ashby, P. D. & Lieber, C. M. Ultra-sensitive imaging and interfacial analysis of patterned hydrophilic SAM surfaces using energy dissipation chemical force microscopy. *J. Am. Chem. Soc.* **127,** 6814 (2005).

39. Martinez, N. F. & García, R. Measuring phase shifts and energy dissipation with amplitude modulation atomic force microscopy. *Nanotechnology* **17,** S167–S172 (2006).

40. Xu, W. S., Wood-Adams, P. M. & Robertson, C. G. Measuring local viscoelastic properties of complex materials with tapping mode atomic force microscopy. *Polymer* **47,** 4798–4810 (2006).

41. Oyabu, N. *et al.* Single atomic contact adhesion and dissipation in dynamic force microscopy. *Phys. Rev. Lett.* **96,** 106101 (2006).

42. Loppacher, C. *et al.* Experimental aspects of dissipation force microscopy. *Phys. Rev. B* **62,** 13674–13679 (2000).

43. Schirmeisen, A. & Hölscher, H. Velocity dependence of energy dissipation in dynamic force microscopy: Hysteresis versus viscous damping. *Phys. Rev. B* **72,** 045431 (2005).

44. Waigh, T. A. Microrheology of complex fluids, *Rep. Prog. Phys.* **68,** 685–742(2005).

45. Gray, T. *et al.* Nanorheological approach for characterization of electroluminescent polymer thin films. *Appl. Phys. Lett.* **83,** 2563–2565 (2003).

46. Reiter, G., Castelein, G., Sommer, J. U., Röttele, A. & Thurn-Albrecht, T. Direct visualization of random crystallization and melting in arrays of nanometer-size polymer crystals. *Phys. Rev. Lett.* **87,** 226101 (2001).

47. Rehse, N., Marr, S., Scherdel, S. & Magerle, R. Three-dimensional imaging of semicrystalline polypropylene with 10 nm resolution. *Adv. Mater.* **17,** 2203–2206 (2005).

48. Wu, W., Matyjaszewski, K. & Kowalewski, T. Monitoring surface thermal transitions of ABA triblock copolymers with crystalline segments using phase contrast tapping mode atomic force microscopy. *Langmuir* **21,** 1143–1148 (2005).

49. Suo, Z. *et al.* HEPES-stabilized encapsulation of Salmonella typhimutium. *Langmuir* **23,** 1365–1374 (2007).

50. Goede, K., Busch, P. & Grundmann, M. Binding specifity of a peptide on semiconductor surfaces. *Nano Lett.* **4,** 2115–2120 (2004).

51. Checco, A., Cai, Y., Gang, O. & Ocko, B. M. High resolution non-contact AFM imaging of liquids onto chemically nanopatterned surfaces. *Ultramicroscopy* **106,** 703–708 (2006).

52. Lysetska M. *et al.* UV light-damaged DNA and its interaction with human replication protein A: an AFM study. *Nucleic Acids Res.* **30,** 2686–2691 (2002).

53. Uchihashi, T., Ando, T. & Yamashita, H. Fast phase imaging in liquids using a rapid scan atomic force microscope. *Appl. Phys. Lett.* **89,** 213112 (2006).

54. Knoll, A., Magerle R. & Krausch, G. Phase behaviour in thin films of cylinder-forming ABA block copolymers. *J. Chem. Phys.* **120,** 1105–1116 (2004).

55. Knoll, A. *et al.* Direct imaging and mesoscale modeling of phase transitions in a nanostructured fluid. *Nature Mater.* **3,** 886–891 (2004).

56. Hahm, J., Lopes, W. A., Jaeger, H. M. & Sibener, S. J. Defect evolution in ultrathin films of polystyrene-*block*-polymethylmethacrylate diblock copolymers observed by atomic force microscopy. *J. Chem. Phys.* **109,** 10111–10114 (1998).

57. Harrison, C. *et al.* Mechanisms of ordering in striped patterns. *Science* **290,** 1558–1561 (2000).

58. Tsarkova, L., Knoll, A. & Magerle, R, Rapid transitions between defect configurations in a block copolymer melt. *Nano Lett.* **6,** 1574–1577 (2006).

59. Xu, J. *et al.* Direct AFM observation of crystal twisting and organization in banded spherulites of chiral poly(3-hydroxybutyrate-*co*-3-hydroxyhexanoate). *Macromolecules* **37,** 4118–4123 (2004).

60. Tamayo, J. Energy dissipation in tapping-mode scanning for microscopy with low quality factors. *Appl. Phys. Lett.* **75,** 3569–3571 (1999).

Competing financial interests
The authors declare no competing financial interests.